

Microdroplet formation in rounded flow-focusing junctions

Shelly Gulati¹ · Kalpana Vijayakumar² · Wilson W. Good¹ · Warren L. Tamayo¹ · Akhil R. Patel¹ · Xize Niu³

Received: 12 August 2015 / Accepted: 15 November 2015 / Published online: 5 January 2016
© Springer-Verlag Berlin Heidelberg 2015

Abstract Herein we report microfluidic droplet formation in flow-focusing geometries possessing varying degrees of rounding. Rounding is incorporated in all four corners (symmetric) or only in the two exit corners (asymmetric). The ratios of the radius of curvature, R , to channel width, w , are varied where $R/w = 0, 0.5$ and 1 . In all cases, monodisperse droplets are produced, with the largest droplets being produced at the junctions with the largest rounding. Junctions without rounding are shown to produce droplets at higher frequencies than those with rounding. Droplet pinch-off position is found to be dependent on both geometry and volumetric flow rates; the location shifts toward the interior of the rounded junctions with increasing oil-to-water flow rate ratios. Accordingly, we find that rounding within microfluidic flow-focusing junctions strongly influences droplet formation. Junction rounding may be deliberate due to the selected fabrication method or occur as an unintended result of microfabrication processes not held to strict tolerances. Indeed, understanding droplet characteristics for those formed in such structures is critical for microfluidic applications where droplet volume or reagent mass must be well controlled. Thus, rounding can be a valuable design parameter when tuning the size and

production frequency for emulsion collection or ensuing downstream operations such as chemical reactions.

Keywords Droplet production · Microfluidics · Flow focusing · Flow instabilities

1 Introduction

Droplet-based microfluidic technologies have received considerable attention as promising novel microfluidic platforms for performing chemical and biological analyses, and have been applied for a variety of purposes, including enzymatic kinetic assays (Song and Ismagilov 2003), cell-free protein expression (Dittrich et al. 2005; Courtois et al. 2008), production of hydrogel beads (Um et al. 2008), formation of microspheres (Chokkalingam et al. 2010), and synthesis of nanomaterials (Lignos et al. 2014; Kumar et al. 2012; Khan et al. 2004).

Aqueous droplets within an oil carrier fluid are generated by leveraging flow instabilities in microfluidic channel structures. As a result, the aqueous phase can be compartmentalized into isolated reactor volumes. Such droplets, which can be dosed with controllable reagent compositions, are characterized by their miniscule volumes (typically from femtoliters to nanoliters), their near identical (monodisperse) size, and their reproducible formation at high frequencies (kHz–MHz) over extended time periods (Theberge et al. 2010).

Leveraging other beneficial operating characteristics of droplet-based microfluidic technologies allows complex chemical or biological experiments to be performed in a highly reproducible and automated manner. For example, precise volumes of distinct reagent droplets can be produced by separate droplet formation elements, flowed into

✉ Shelly Gulati
sgulati@pacific.edu

¹ School of Engineering and Computer Science, Bioengineering Program, University of the Pacific, Stockton, CA, USA

² Department of Chemistry, Imperial College London, London, UK

³ Faculty of Engineering and the Environment, University of Southampton, Southampton, UK

a common channel stream, and controllably merged (Niu et al. 2008; Bremond et al. 2008; Um et al. 2008) to initiate volume-controlled reactions (Chokkalingam et al. 2010). The merging of droplets allows initiation of a reactive process, with droplet contents being rapidly mixed by internal flow circulation or chaotic advection (Tice et al. 2003; Song et al. 2003).

Exact control of droplet volume (or size) and temporal management of the droplet production process are essential to performing volume-controlled reactions. Thorough characterization of droplet volume may also be critical for other downstream processes, such as precise dilution by merging droplets (Niu et al. 2011) and volume control at a droplet splitting element (Link et al. 2004). As such, attention must be focused on the microfluidic elements used to form droplets and the influence, if any, of modifications to those elements on the droplet formation process and droplet characteristics.

In microfluidic channels, relatively large diameter droplets (plugs) can be formed at single droplet units by co-flowing, cross-flowing, and flow focusing (Engl et al. 2008; Christopher and Anna 2007), in parallel units by straight-through microchannels (Kobayashi et al. 2008, 2009), and in microchannel arrays with steps (Sugiura et al. 2002; Liu et al. 2005). The numerous microfluidic methods for producing uniform droplets flows via single droplet formation and parallel droplet formation have been comprehensively reviewed elsewhere (Engl et al. 2008; Christopher and Anna 2007; van Dijke et al. 2009).

Flow-focusing elements are perhaps the most versatile and widely used geometry for droplet generation, where two streams of continuous phase converge with a central stream of the dispersed phase and are compelled to flow through a narrow orifice. Confinement then causes the central stream to destabilize and segment (Romero and Abate 2012). Specifically, as the dispersed phase fluid front enters and fills the junction, the continuous phase flow is blocked. The resulting upstream pressure squeezes the dispersed phase to a thinning neck that eventually pinches off into a drop. According to this plug and squeeze mechanism, droplet characteristics in flow-focusing geometries are strongly influenced by the continuous phase flow rate (Lee et al. 2009; Garstecki et al. 2005). These shear-based junctions are desirable for size control applications because of their high monodispersity (Xu et al. 2005; Christopher and Anna 2007; van Dijke et al. 2009; Mulligan and Rothstein 2012).

Early flow-focusing geometry structures, such as those described by Anna et al. (2003), were comprised of three parallel inlet channels (two continuous streams flank a dispersed stream) that converged to a single channel sized to be as large as the combined inlet widths. Droplets form as the fluids are forced through a narrow gap connected to a large downstream channel. More recently, flow-focusing

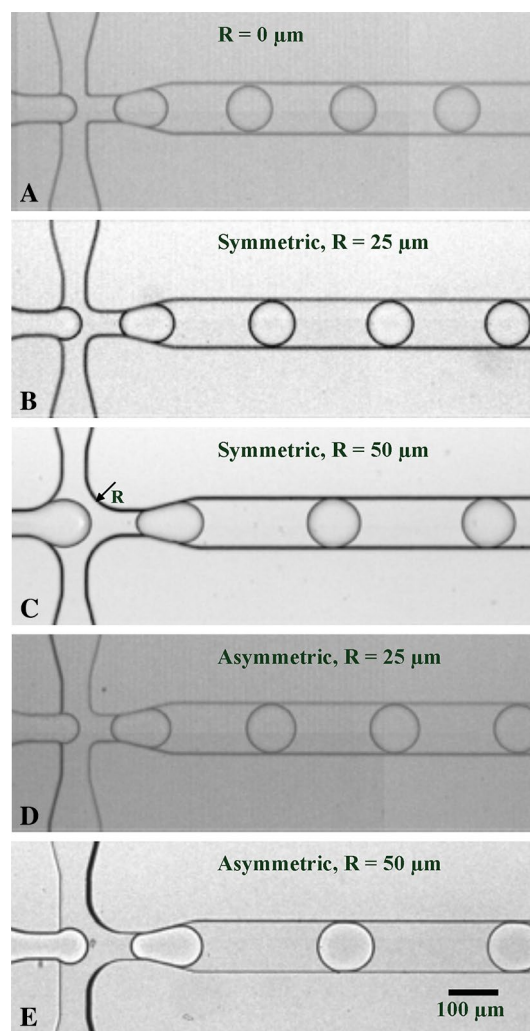


Fig. 1 Representative images of the five variant flow-focusing devices: **a** flow-focusing junction with no corner rounding, radius of curvature $R = 0 \mu\text{m}$; flow-focusing junction with symmetric rounding in all the four corners with radii of curvature **b** $R = 25 \mu\text{m}$ and **c** $R = 50 \mu\text{m}$; and flow-focusing junction with asymmetric rounding of the two downstream corners with radii of curvature **d** $R = 25 \mu\text{m}$ and **e** $R = 50 \mu\text{m}$. Each device is producing droplets at a flow rate ratio $Q_r = 3$

geometries have commonly consisted of input channels joined at right angles to form a cross-junction (Fig. 1). The exit channel is positioned directly opposite the dispersed phase inlet, with the continuous phase being contained in the other channels. Some “right-angle” cross-junction designs have the inlet channel widths locally reduced and then expanded at the exit of the junction (Abate et al. 2009; Niu et al. 2008). Others with rounded junction corners have also been fabricated as a result of hot embossing techniques (Subramanian et al. 2011; Wu et al. 2009). Due to such geometric differences (as well as fluid system differences), each flow-focusing device must be individually calibrated for operation and droplet characteristics. For example, a

study of droplet formation in flow-focusing junctions with variable injection angles (15°, 30°, 45°, 60°, 90° and 120°) demonstrated the production of different drop sizes under identical flow conditions (Liu et al. 2007).

In reality, very sharp corner features can be difficult to achieve for some commonly employed microfabrication techniques. For example, when using soft lithographic methods to produce elastomeric devices, both the fabrication of the mold and the ensuing replication steps may result in feature rounding. Micropattern transfer to SU-8 epoxy molds is exquisitely sensitive to UV exposure dose, with underexposure causing rounded corners (Wong et al. 2014). Rounding can also occur as a result of light scattering during exposure, especially for thick layers (>1 μm) of photoresist and imperfect contact between the mask and mold (del Campo and Greiner 2007). Even if perfect exposure allows the generation of sharp corners on the master mold, the replica elastomer (after release) will adopt an equilibrium shape (defined by material elasticity and interface tension) that is characterized by minute rounding (Gordan et al. 2008; Odom et al. 2002). Similarly, sharp corners are difficult to fabricate by hot embossing due to limitations in micromilled mold resolution (Griffiths et al. 2010; Becker et al. 1998), since the radius of curvature is restricted to the radius of the milling bit (Guber et al. 2004). It should be noted that near 90° features can be realized using UV-LIGA techniques to produce molds; however, slight rounding is almost unavoidable (Guber et al. 2004).

The presence or absence of geometric rounding at a fluidic junction is expected to influence the local flow environment differently. For example, numerical simulations of a continuous flow electrophoresis device by Hupert et al. (2007) found that there was an increase in volume of injection plugs due to rounded corners with radius of curvature R , at a cross-junction of width w , compared to a “sharp” junction, with the sample plug size increasing 10–20 % for $R/w < 0.5$ and ~50 % for $R/w = 1$ (Hupert et al. 2007).

In this regard, an interesting question that remains unanswered is the influence of deviations in rounding of corners in a flow-focusing junction on the droplet formation. Herein, we systematically explore the formation of aqueous droplets (in a continuous oil phase) in flow-focusing designs that have identical channel dimensions; however, the radii of curvature in the corners of the cross-shaped junction were adjusted to $R/w = 0.5$ and 1 and compared to structures with no rounding ($R/w = 0$). Rounding was positioned either in all four corners (symmetric) or in only the two downstream corners (asymmetric). A symmetric junction with $R/w = 0.5$ mimics a junction that could be fabricated by underexposure of an SU-8 mold for soft lithography. Symmetric junctions with $R/w = 1$ mimic devices commonly fabricated by hot embossing using micromilled

molds. The asymmetric junctions (where $R/w = 0.5$ and 1) isolate the effect of downstream rounding. These are contrasted with junctions designed with minimal rounding ($R/w \approx 0$) that are typically produced using soft lithography. Droplet formation and droplet characteristics in these junctions are systematically studied under identical flow conditions.

2 Experimental methods

Five flow-focusing junctions were compared in this study and are shown in Fig. 1. Broad geometric features for the five devices were maintained for each junction, but the degree of rounding of the entrance and exit corners of the cross-junction was varied to isolate the effects of these differences on droplet formation and droplet characteristics. For each cross-shaped junction design, fluid enters via three inlet channels that are 100 μm in width and gradually contract to 50 μm. The dispersed phase fluid enters horizontally, and the two channels with the continuous phase fluid join perpendicularly. Droplets within the carrier fluid exit through the opposite horizontal channel that is initially 50 μm wide and gradually expands to 100 μm. The channel depth for all channels is 50 μm.

The flow-focusing junctions differ in the locations and radius of curvature of rounded corners at the junction. The radius of curvature was either 0 μm (i.e., not rounded), 25 or 50 μm. Additionally, rounding was either in all four corners (symmetric) or only in the two downstream corners with no rounding in the upstream corners (asymmetric). The junction with $R = 0$ μm resembles a standard flow-focusing junction fabricated with the sharpest corners possible using traditional soft lithographic techniques.

Figure 1 provides images of the five flow-focusing junction geometries used. Figure 1a shows the flow-focusing junction with no corner rounding ($R = 0$ μm). Figure 1b, c illustrates the flow-focusing junction with symmetric rounding ($R = 25$ and 50 μm respectively). Figure 1d, e shows flow-focusing junctions with asymmetric rounding of the two downstream corners ($R = 25$ and $R = 50$ μm, respectively). The measured downstream channel widths w_d ($98.6 \mu\text{m} < w_d < 101.7 \mu\text{m}$) and measured cross-junction widths w ($47.7 \mu\text{m} < w < 50.8 \mu\text{m}$) for the junction designs vary slightly, which is likely due to differences introduced during the fabrication process.

The flow-focusing junctions compared in this study were fabricated in polydimethylsiloxane (PDMS) using standard soft lithography techniques (Xia and Whitesides 1998). PDMS base and curing agent (Sylgard184, Dow Corning, Coventry UK) were prepared at a ratio of 10:1 (w/w) and cured at 70 °C over the SU-8 patterned silicon master molds. The molded PDMS devices were divided and peeled

off the master. A biopsy punch (Kai Europe GmbH, Solingen, Germany) was used to introduce through-holes to the PDMS devices for off-chip access to inlet and outlet reservoirs. Sequentially, the PDMS devices were permanently adhered to glass slides via plasma bonding.

Portex[®] fine bore tubing (0.38 mm ID, 1.09 OD, Smiths Medical International Ltd, Kent, UK) was used for inlet and outlet tubing for all of the flow-focusing devices, ensuring equivalent contributions to device operation. One end of each piece of tubing was inserted directly into the bored through-holes in the PDMS device. The other end of the inlet tubing was connected to a 1 ml BD Plastipak syringe (VWR, UK) using syringe needles (BD Microlance[™] 3 Nr.18, VWR, UK), with the other end of the outlet tubing being directed to a waste container.

For all experiments, the carrier fluid was a mixture of a fluorinated oil, Fluorinert FC-3283 (3M, Bracknell, UK), and an electronic coating liquid, Novec[™] EGC-1700 (3M, Bracknell, UK). Deionized water served as the dispersed phase. This microdroplet system was selected because it is an example of a platform that is relevant for biological or chemical experiments. The coating liquid (EGC-1700) provides a thin film coating along the walls, which prevents adsorption (Srisa-Art et al. 2009). Fluorinated oils are beneficial for oxygen permeability and immiscibility with organic compounds (Theberge et al. 2010).

Two precision syringe pumps (PHD 2000, Harvard Apparatus, Cambridge, MA, USA) were used to independently deliver the two fluids to the device at constant volumetric flow rates. The flow of the dispersed phase Q_d was held constant for all experiments at 1 $\mu\text{l}/\text{min}$, and the flow of the continuous phase Q_c (the sum of both vertical inlet streams at the junction) was varied from 1 to 8 $\mu\text{l}/\text{min}$. The formation of aqueous droplets in oil for flow rate ratios $1 < Q_r = Q_c/Q_d < 8$ was examined in the five flow-focusing devices. A high-speed CMOS camera (Phantom[®], v649, Vision Research, Bedford, UK) was used to acquire video microscopy images under 10 \times magnification. Five to seven runs were conducted for each test condition in all the flow-focusing geometries with the oil and water flows stopped in between and returned to stable, periodic flows before collecting new video images. The number of drops formed over the recorded time was quantified for each run as the droplet production frequency. Other droplet characteristics were found by processing recorded images using Image J software (NIH, Bethesda, MD, USA). Droplet diameter or the centerline length of the formed droplet in the downstream channel was measured for each condition. Additionally, the pinch-off position or the distance along the flow direction from the upstream wall of the 50- μm -wide section of the oil inlet to the position where the dispersed fluid thread is thinnest just prior to pinch-off was determined for each flow rate ratio and flow-focusing geometry.

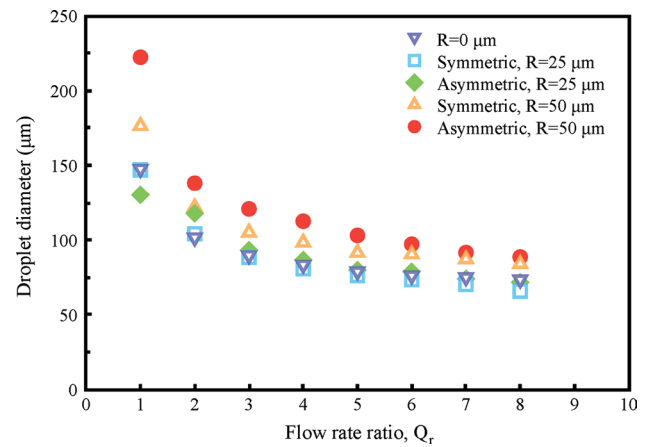


Fig. 2 Average droplet diameter as a function of flow rate ratio Q_r for the five variant flow-focusing devices

3 Results and discussion

Figure 1 contains images of the five variants of the flow-focusing devices whose junction geometries differ in their radii of curvature R and corners of rounding (either symmetric or asymmetric). The droplets in each geometry are formed at $Q_r = 3$. These images clearly report the differences in droplet size and frequency of generation in each of the flow-focusing geometries under identical flow rate conditions.

The droplet formation processes in each device share the same broad features of a plug and squeeze mechanism. The water enters the junction migrating toward the exit channel and expanding into the two continuous phase oil inlets. Eventually, the water plugs the junction, preventing the flow of oil. The rise in pressure of the oil phase squeezes the water until it ultimately pinches off a water droplet. The droplets formed are plugs that have a diameter larger than the junction channel width w . Differences between the flow-focusing geometries appear in the size of the water bulge in the junction region prior to plugging. Larger rounding geometries provide more space for the growth of the projection, with the greatest intrusion of volume occurring for the symmetric, $R = 50 \mu\text{m}$ junction.

The average droplet diameters as a function of flow rate ratio for each flow-focusing geometry are presented in Fig. 2. For each device, drop size varies strongly as a function of flow rate ratio; drop diameter halves across an eightfold increase in flow rate ratio. Many similar observations of droplet size reduction with increasing flow rate ratio have been reported previously (Tan et al. 2006; Tice et al. 2003; Mulligan and Rothstein 2012). The uniformity of drop sizes for a given condition can be described by the coefficient of variation (CV) or the ratio of the standard

deviation and the average drop diameters. For all flow conditions and geometries, the CV was 2 % or lower, except for two conditions: asymmetric, $R = 25 \mu\text{m}$ at $Q_r = 2$ and asymmetric, $R = 50 \mu\text{m}$ at $Q_r = 1$ with CVs = 4 and 5 %, respectively. The higher CVs occur due to variation in droplet sizes during different trials at the same flow rate ratio. The continuous phase may experience more pronounced pressure perturbations between runs for the low flow rate conditions due to the asymmetry at the junction. This in turn would deviate the pinching process of the dispersed phase. The variance in the plug and squeeze mechanism will result in modest differences in droplet diameter. Nevertheless, the drop diameters for all flow conditions and geometries are found to have narrow size distributions, which define monodisperse populations according to the National Institute of Standards and Technology definition (Jillavenkatesa et al. 2001).

Figure 2 demonstrates that for both the symmetric and asymmetric geometries, larger drop sizes are obtained for the larger rounding cases ($R = 50 \mu\text{m}$) compared with their smaller rounding counterparts ($R = 25 \mu\text{m}$) and the non-rounded geometry ($R = 0 \mu\text{m}$) for all Q_r values tested. Additionally, the asymmetric, $R = 50 \mu\text{m}$ junction creates larger droplets than the symmetric, $R = 50 \mu\text{m}$ junction for each Q_r condition. The difference in size is largest for $Q_r = 1$ and drops off with increased Q_r . This difference can be observed by comparing the drop diameters produced for the case of $Q_r = 3$ in Fig. 1c, e. Figure 2 also reveals comparable average drop sizes for the $R = 0 \mu\text{m}$ and symmetric, $R = 25 \mu\text{m}$ geometry for all Q_r and for the asymmetric, $R = 25 \mu\text{m}$ geometry when $Q_r > 2$. Images in Fig. 1a, b, and d show that comparable drop diameters are obtained for the smaller and no rounding junctions for the $Q_r = 3$ case. The differences in the size observed at $Q_r = 1$ and $Q_r = 2$ for these geometries are likely to be due to the variation in the droplet formation process at these low flow rate ratios.

The frequency of droplet production as a function of flow rate ratio for each flow-focusing geometry is illustrated in Fig. 3. At the lowest flow rate ratio, droplet production frequencies for all geometries except the asymmetric, $R = 25 \mu\text{m}$ junction are similar ranging between ~ 16 and 23 Hz at $Q_r = 1$. The asymmetric, $R = 25 \mu\text{m}$ junction has higher drop production frequency of about 37 Hz . A rise in droplet production frequency occurs with increasing flow rate ratio for all geometries, with the highest frequencies occurring for the $R = 0 \mu\text{m}$ geometry. The asymmetric and symmetric, $R = 25 \mu\text{m}$ junctions have comparable frequencies at $Q_r > 1$. The slowest droplet formation frequencies are observed for the $R = 50 \mu\text{m}$ junctions, with the symmetric geometry producing droplets at a lower frequency than the asymmetric shape. These differences in the formation frequency for the devices are apparent from

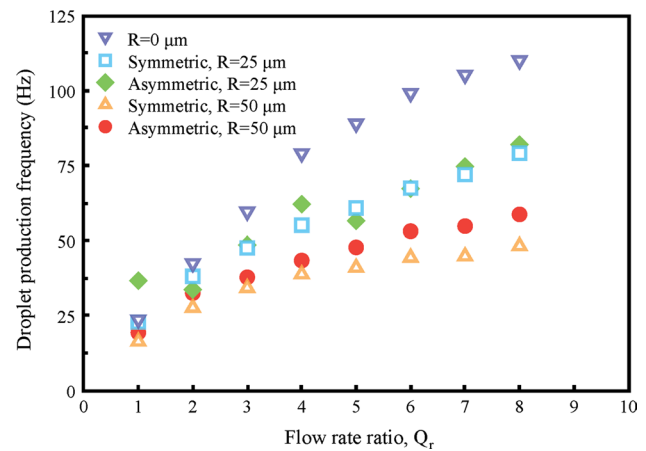


Fig. 3 Droplet production frequency as a function of flow rate ratio Q_r for the five variant flow-focusing devices

the spacing of the droplet trains in the images in Fig. 1 for $Q_r = 3$. At the highest flow rate ratio $Q_r = 8$, droplets in the junction with no rounding are formed more than twice as frequently as drops in the symmetric, $R = 50 \mu\text{m}$ device (Fig. 3) with an $\sim 20\%$ reduction in the diameter (Fig. 2).

Images of droplet formation just before pinch-off are presented in Fig. 4 for the symmetric and asymmetric geometries at $Q_r = 1$ and $Q_r = 7$. This is the final stage of the plugging–squeezing process of drop formation in flow-focusing devices (Romero and Abate 2012). Differences in the location of pinch-off, where the droplet thread is thinnest within the junction region, and droplet spacing are revealed. Additionally, the comparative size of droplets by geometry and flow rate ratio is evident. Figure 5 shows the evolution of pinch-off position with flow rate ratio for each geometry. We estimate the uncertainty in measuring the pinch-off position is 2 pixels or $\sim 3.2 \mu\text{m}$. The largest standard deviations s_p were obtained for the symmetric, $R = 25 \mu\text{m}$ case which were slightly larger than the estimated uncertainty ($3.46 < s_p < 3.75$ for $5 < Q_r < 7$).

The pinch-off location is observed to be both geometry and flow rate ratio dependent (Fig. 5). The pinch-off positions for the $R = 0 \mu\text{m}$ junction are nearly the same across flow rate ratios; the average values all fall within the measurement uncertainty. This is also obtained for the asymmetric, $R = 25 \mu\text{m}$ junction; however, close inspection of Fig. 4c, d reveals a pinch-off location for $Q_r = 7$ that is slightly upstream of the $Q_r = 1$ image. This shift in pinch-off location at the lowest flow rate ratio compared with the pinch-off for the rest of the range is more evident for the asymmetric, $R = 50 \mu\text{m}$ junction (cf. Figs. 4g, h; 5). A decay in pinch-off position (i.e., the shift of the position toward the interior of the junction) with increasing flow rate ratio across the entire range is observed for the symmetric, $R = 25 \mu\text{m}$ junction (cf. Figs. 4a, b, 5) and is

Fig. 4 Representative images of droplet formation just prior to pinch-off in the four rounded flow-focusing devices at two different flow rate ratios: symmetric flow-focusing junction with radius of curvature $R = 25 \mu\text{m}$ at **a** $Q_r = 1$ and **b** $Q_r = 7$; asymmetric flow-focusing junction with radius of curvature $R = 25 \mu\text{m}$ at **c** $Q_r = 1$ and **d** $Q_r = 7$; symmetric flow-focusing junction with radius of curvature $R = 50 \mu\text{m}$ at **e** $Q_r = 1$ and **f** $Q_r = 7$; asymmetric flow-focusing junction with radius of curvature $R = 50 \mu\text{m}$ at **g** $Q_r = 1$ and **h** $Q_r = 7$

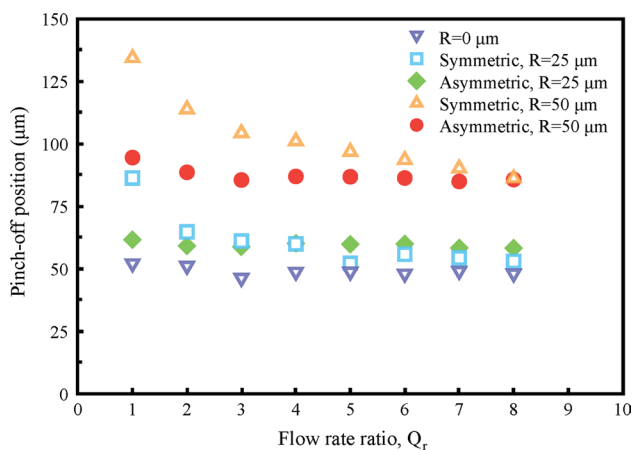
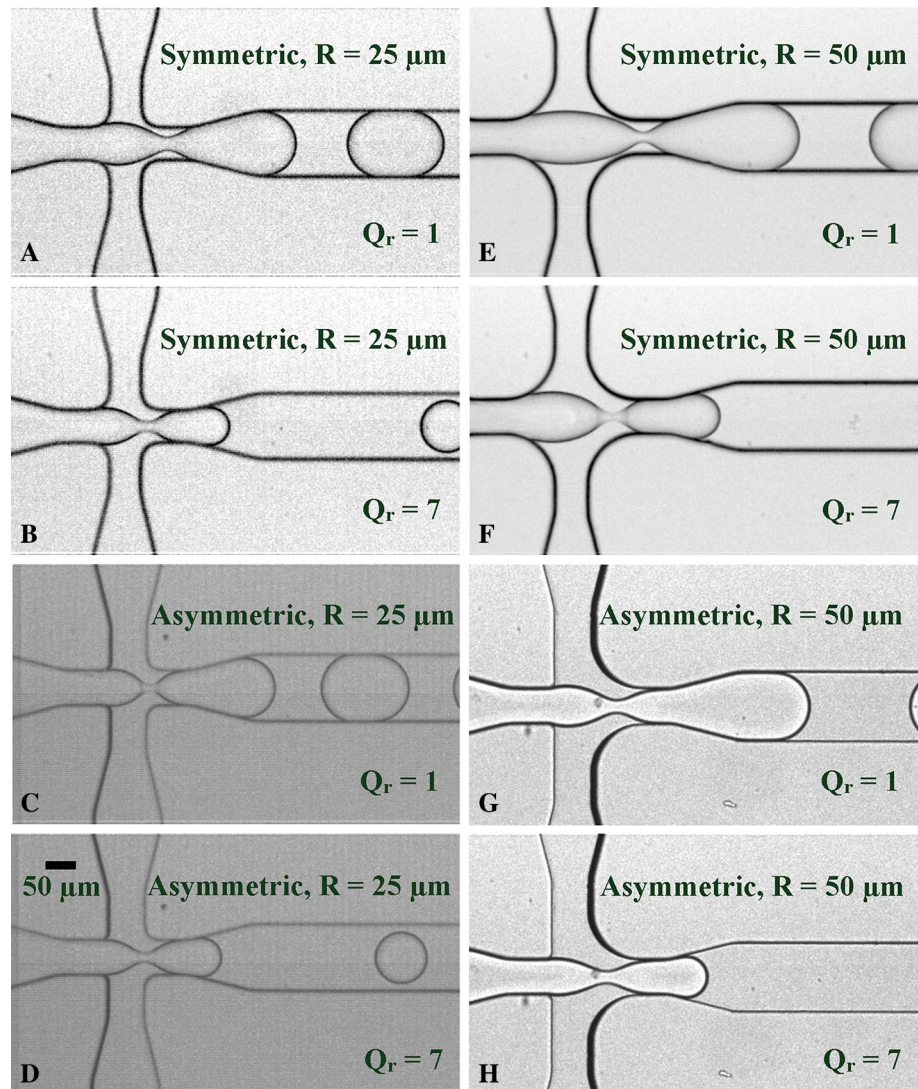
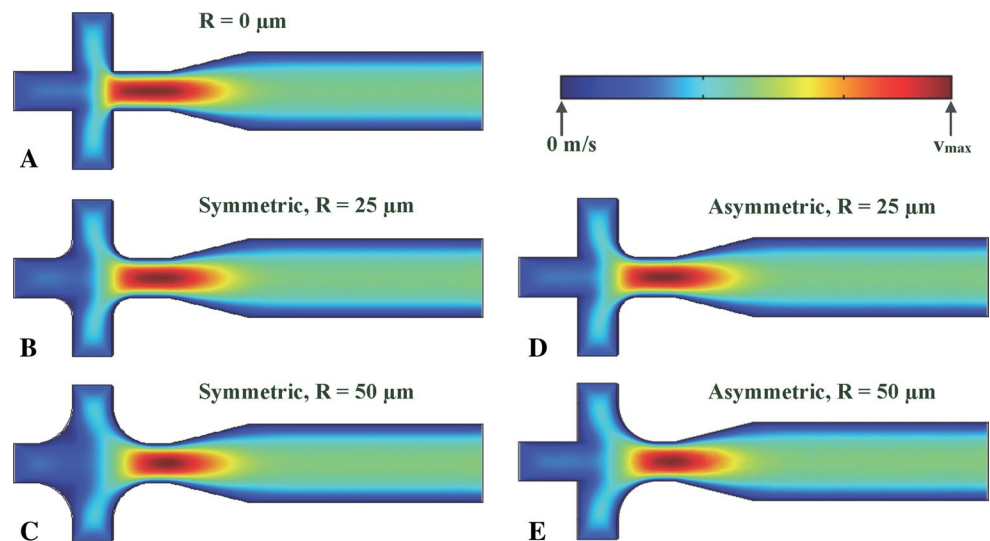


Fig. 5 Pinch-off position as a function of flow rate ratio Q_r for the five variant flow-focusing devices

most striking for the symmetric, $R = 50 \mu\text{m}$ junction (cf. Figs. 4e, f, 5). For these geometries, at the lowest flow rate ratio, $Q_r = 1$, the pinch-off occurs past the rounded section and into the $50\text{-}\mu\text{m}$ -wide section of the downstream channel (Fig. 4a, e).

Tan et al. (2006) reported that the droplet pinch-off location could be focused to a single point in a flow-focusing geometry with a nozzle-shaped exit. In this geometry, the fluid is immediately expanded into a triangularly shaped reservoir at the exit of the junction. At the pinch-off location, the fluid flow experiences maximum velocity and a sharp velocity gradient along the flow direction (Tan et al. 2006). This contrasts from the junctions in this study whose junction exit is comprised of a short straight channel that is gradually expanded into another straight channel. Single-phase three-dimensional flow simulations at the inlet flow rates were conducted using *Comsol Multiphysics 4.3b* for the five flow-focusing geometries in this study to quantify

Fig. 6 Velocity fields computed using *Comsol Multiphysics 4.3b* for single-phase flow in the five variant flow-focusing devices at $Q_r = 3$: **a** flow-focusing junction with no corner rounding, radius of curvature $R = 0 \mu\text{m}$; flow-focusing junction with symmetric rounding in all the four corners with radii of curvature **b** $R = 25 \mu\text{m}$ and **c** $R = 50 \mu\text{m}$; and flow-focusing junction with asymmetric rounding of the two downstream corners with radii of curvature **d** $R = 25 \mu\text{m}$ and **e** $R = 50 \mu\text{m}$



the velocity fields. The single-phase simulations estimate a comparable relative velocity distribution to that experienced by the continuous phase of the two-phase flow (Tan et al. 2006). Figure 6 shows the velocity fields that are calculated for inlet flows of a Newtonian fluid at $Q_r = 3$. The simulations reveal that the maximum velocity v_{max} occurs over the entire section of the downstream channel with the narrowest width (the length of this section shortens as the radius of curvature is increased) and a velocity gradient across the flow direction is not present in this section. This supports the experimental results in this study that indicate the droplet breakup position varies along the channel junction depending on the flow conditions.

Studying the droplet formation process in junctions with varying rounding geometries elucidates the effect on droplet characteristics if device fabrication is not held within strict tolerances. Larger droplets than expected may be formed due to rounded corners formed during fabrication. If droplet volumes or concentrations need to be exactly controlled, downstream operations may be complicated or even compromised.

4 Conclusions

The formation of monodisperse aqueous microdroplets in oil across a range of oil-to-water flow rate ratios was studied in five flow-focusing geometries that varied in their radii of curvature and if all four corners were rounded (symmetric) or if only the two exit corners were rounded (asymmetric). Due to the nature of some fabrication methods, symmetric rounding is unavoidable in the majority of microfluidic structures. Asymmetric geometries isolate the influence of rounding in the downstream exit.

This study shows that the droplet formation and droplet characteristics are sensitive to slight variations in the flow-focusing junction design. Accordingly, intentional design of junction rounding can be utilized to tune the size and production frequency of the droplets for collection or subsequent operations. Conversely, if fabrication cannot be held within strict tolerances and unintended rounding occurs, expected droplet volumes will not be obtained. This may be problematic if volume control (or alternately mass control) is needed for operations such as droplet dilution, droplet splitting, or chemical reactions, in which case, either feedback altering the flow rate of the continuous phase is needed to adjust the size of droplets or new droplet formation approaches should be employed, for example (Gielen et al. 2013). Additionally, the continuous phase viscosity could be modified to regulate the size of droplets in the rounded geometries. If a continuous phase with higher viscosity is used, the droplet size is expected to increase due to the slowing of thread thinning and pinch-off process as compared to use of a lower viscosity continuous phase. Additionally, at higher continuous phase viscosity, the droplet sizes produced are less sensitive to flow rate ratio changes (Nie et al. 2008). This predictability could be advantageous for volume-controlled operations.

By utilizing the defined dependence of drop size on the flow rate ratio and junction rounding, production of droplets of dissimilar volumes can readily be produced. This can be beneficial for applications in reaction chemistry. Flow-focusing droplet generators can be flow-controlled individually or operated in parallel. The precisely controlled, yet distinctly different volume drops could then be transported in conduit channels of identical width and depth and joined into a single stream for downstream merging in a reaction chip.

Systematic rounding at flow-focusing junctions can also find use in large-scale production of droplets. High output droplet production on a microfluidic platform can be achieved by parallel droplet generation with straightforward external connections (Mulligan and Rothstein 2012; Li et al. 2007). Deliberate and varied rounding at each flow-focusing element in the parallel scheme could allow the production of a precisely polydisperse distributions of droplets via a facile flow format with one continuous fluid input and one dispersed phase input. Controlled distributions of emulsion droplets may be beneficial for a variety of industrial applications (Anna et al. 2003).

Acknowledgments This work was supported in part by the RCUK Microdroplets Basic Technology Project (EP/D048664/1). The authors would like to thank Joshua B. Edel and Andrew J. deMello for useful discussions and the use of their cleanroom facilities to fabricate devices. SG and WG would like to acknowledge support from the School of Engineering and Computer Science at University of the Pacific.

References

- Abate AR, Poitzsch A, Hwang Y, Lee J, Czerwinska J, Weitz DA (2009) Impact of inlet channel geometry on microfluidic drop formation. *Phys Rev E* 80:026310
- Anna SL, Bontoux N, Stone HA (2003) Formation of dispersions using “flow focusing” in microchannels. *Appl Phys Lett* 82:364–366
- Becker H, Dietz W, Dannberg P (1998) Microfluidic manifolds by polymer hot embossing for μ -TAS applications. In: Harrison DJ, van den Berg A (eds) *Proceedings of micro total analysis systems*. Kluwer, Dordrecht, pp 253–256
- Bremont N, Thiam AR, Bibette J (2008) Decompressing emulsion droplets favors coalescence. *Phys Rev Lett* 100:024501
- Chokkalingam V, Weidenhof B, Krämer M, Maier WF, Herminghaus S, Seemann R (2010) Optimized droplet-based microfluidics scheme for sol–gel reactions. *Lab Chip* 10:1700–1705
- Christopher GF, Anna SL (2007) Microfluidic methods for generating continuous droplet streams. *J Phys D Appl Phys* 40:R319–R336
- Courtois F, Olguin LF, Whyte G, Bratton D, Huck WTS, Abell C, Hollfelder F (2008) An integrated device for monitoring time-dependent in vitro expression from single genes in picolitre droplets. *ChemBioChem* 9:439–446
- del Campo A, Greiner C (2007) SU-8: a photoresist for high-aspect-ratio and 3D submicron lithography. *J Micromech Microeng* 17:R81–R95
- Dittrich P, Jahnz M, Schwille P (2005) A new embedded process for compartmentalized cell-free protein expression and on-line detection in microfluidic devices. *ChemBioChem* 6:811–814
- Engl W, Backov R, Panizza P (2008) Controlled production of emulsions and particles by milli- and microfluidic techniques. *Curr Opin Colloid Interface Sci* 13:206–216
- Garstecki P, Stone HA, Whitesides GM (2005) Mechanism for flow-rate controlled breakup in confined geometries: a route to monodisperse emulsions. *Phys Rev Lett* 94:164501
- Gielen F, van Vliet L, Koproswi BT, Devenish SRA, Fischlechner M, Edel JB, Niu X, deMello AJ, Hollfelder F (2013) A fully unsupervised compartment-on-demand platform for precise nanoliter assays of time-dependent steady-state enzyme kinetics and inhibition. *Anal Chem* 85:4761–4769
- Gordan OD, Persson BNJ, Cesa CM, Mayer D, Hoffmann B, Dieluwweit S, Merkel R (2008) On pattern transfer in replica molding. *Langmuir* 24:6636–6639
- Griffiths C, Bigot S, Brousseau E, Worgull M, Hecke M, Nestler J, Auerswald J (2010) Investigation of polymer inserts as prototyping tooling for micro injection moulding. *Int J Adv Manuf Technol* 47:111–123
- Guber AE, Hecke M, Herrmann D, Muslija A, Saile V, Eichhorn L, Gietzelt T, Hoffman W, Hauser PC, Tanjanywa J, Gerlach A, Gottschlich N, Knebel G (2004) Microfluidic lab-on-a-chip systems based on polymers—fabrication and application. *Chem Eng J* 101:447–453
- Hupert ML, Guy WJ, Llopis SD, Shadpour H, Rani S, Nikitopoulos DE, Soper SA (2007) Evaluation of micromilled metal mold masters for the replication of microchip electrophoresis devices. *Microfluid Nanofluid* 3:1–11
- Jillavenkatesa A, Dapkunas SJ, Lum L-SH (2001) Particle size characterization. Special Publication 960-1. National Institute of Standards and Technology, Washington
- Khan SA, Gunther A, Schmidt MA, Jensen KF (2004) Microfluidic synthesis of colloidal silica. *Langmuir* 20:8604–8611
- Kobayashi I, Takano T, Maeda R, Wada Y, Uemura K, Nakajima M (2008) Straight-through microchannel devices for generating monodisperse emulsion droplets several microns in size. *Microfluid Nanofluid* 4:167–177
- Kobayashi I, Murayama Y, Kuroiwa T, Uemura K, Nakajima M (2009) Production of monodisperse water-in-oil emulsions consisting of highly uniform droplets using asymmetric straight-through microchannel arrays. *Microfluid Nanofluid* 7:107–119
- Kumar K, Nightingale AM, Krishnadasan SH, Kamaly N, Wylenzinska-Arridge M, Zeissler K, Branford WR, Ware E, deMello AJ, deMello JC (2012) Direct synthesis of dextran-coated superparamagnetic iron oxide nanoparticles in a capillary-based droplet reactor. *J Mater Chem* 22:4704–4708
- Lee W, Walker LM, Anna SL (2009) Role of geometry and fluid properties in droplet and thread formation processing in planar flow focusing. *Phys Fluids* 21:032103
- Li W, Young EWK, Seo M, Nie Z, Garstecki P, Simmons CA, Kumacheva E (2007) Simultaneous generation of droplets with different dimensions in parallel integrated microfluidic droplet generators. *Soft Matter* 4:258–262
- Lignos I, Protesescu L, Stavakis S, Piveteau L, Speirs MJ, Loi MA, Kovalenko MV, deMello AJ (2014) Facile droplet-based microfluidic synthesis of monodisperse IV–VI semiconductor nanocrystals with coupled in-line NIR fluorescence detection. *Chem Mater* 26:2975–2982
- Link DR, Anna SL, Weitz DA, Stone HA (2004) Geometrically mediated breakup of drops in microfluidic devices. *Phys Rev Lett* 92:054503
- Liu H, Nakajima M, Nishi T, Kimura T (2005) Effect of channel structure on preparation of a water-in-oil emulsion by polymer microchannels. *Eur J Lipid Sci Technol* 107:481–487
- Liu K, Zhao L-B, Zeng Q, Guo Z-X, Liu J, Zhao X-Z (2007) Injection angle dependence in flow focusing based droplet formation. In: 1st international conference on bioinformatics and biomedical engineering (ICBBE), pp. 1121–1124
- Mulligan MK, Rothstein JP (2012) Scale-up and control of droplet production in coupled microfluidic flow-focusing geometries. *Microfluid Nanofluid* 13:65–73
- Nie Z, Seo M, Xu S, Lewis PC, Mok M, Kumacheva E, Whitesides GM, Garstecki P, Stone HA (2008) Emulsification in a microfluidic flow-focusing device: effect of the viscosities of the liquids. *Microfluid Nanofluid* 5:585–594
- Niu X, Gulati S, Edel JB, deMello AJ (2008) Pillar-induced droplet merging in microfluidic circuits. *Lab Chip* 8:1837–1841
- Niu X, Gielen F, Edel JB, deMello AJ (2011) A microdroplet dilutor for high-throughput screening. *Nat Chem* 3:437–442

- Odom TW, Love JC, Wolfe DB, Paul KE, Whitesides GM (2002) Improved pattern transfer in soft lithography using composite stamps. *Langmuir* 18:5314–5320
- Romero PA, Abate AR (2012) Flow focusing geometry generates droplets through a plug and squeeze mechanism. *Lab Chip* 12:5130–5132
- Song H, Ismagilov RF (2003) Milliseconds kinetics on a microfluidic chip using nanoliters of reagents. *J Am Chem Soc* 125:14613–14619
- Song H, Tice JD, Ismagilov RF (2003) A microfluidic system for controlling reaction networks in time. *Angew Chem Int Ed* 42:768–772
- Srisa-Art M, Bonzani IC, Williams A, Stevens MM, deMello AJ, Edel JB (2009) Identification of rare progenitor cells from human periosteal tissue using droplet microfluidics. *Analyst* 134:2239–2245
- Subramanian B, Kim N, Lee W, Spivak DA, Nikitopoulos DE, McCauley RL, Soper DA (2011) Surface modification of droplet polymeric microfluidic devices for the stable and continuous generation of aqueous droplets. *Langmuir* 27:7949–7957
- Sugiura S, Nakajima M, Seki M (2002) Effect of channel structure on microchannel emulsification. *Langmuir* 18:5708–5712
- Tan Y-C, Cristini V, Lee AP (2006) Monodisperse microfluidic droplet generation by shear focusing microfluidic device. *Sens Actuators B* 114:350–356
- Theberge AB, Courtois F, Schaerli Y, Fischlechner M, Abell C, Holfelder F, Huck WTS (2010) Microdroplets in microfluidics: an evolving platform for discoveries in chemistry and biology. *Angew Chem Int Ed* 49:5846–5868
- Tice JD, Song H, Lyon AD, Ismagilov RF (2003) Formation of droplets and mixing in multiphase microfluidics at low values of the Reynolds and capillary numbers. *Langmuir* 19:9127–9133
- Um E, Lee D-S, Pyo H-B, Park J-K (2008) Continuous generation of hydrogel beads and encapsulation of biological materials using a microfluidic droplet-merging channel. *Microfluid Nanofluid* 5:541–549
- van Dijke K, Veldhuis G, Schroen K, Boom R (2009) Parallelized edge-based droplet (EDGE) devices. *Lab Chip* 9:2824–2830
- Wong S, Guo W-H, Hoffecker I, Wang Y-L (2014) Preparation of a micropatterned rigid-soft composite substrate for probing cellular rigidity sensing. In: Piel M, Thery M (eds) *Methods in cell biology: micropatterning in cell biology part C*, vol 121. Elsevier, Oxford, pp 3–15
- Wu N, Zhu Y, Brown S, Oakeshott J, Peat TS, Surjadi R, Easton C, Leech PW, Sexton BA (2009) A PMMA microfluidic droplet platform for in vitro protein expression using crude *E. Coli* S30 extract. *Lab Chip* 9:3391–3398
- Xia Y, Whitesides GM (1998) Soft lithography. *Angew Chem Int Ed* 37:550–575
- Xu S, Nie Z, Seo M, Lewis P, Kumacheva E, Stone HA, Garstecki P, Weibel DB, Gitlin I, Whitesides GM (2005) Generation of monodisperse particles by using microfluidics: control over size, shape, and composition. *Angew Chem Int Ed* 44:724–728